

# Measurement-based Simulation of Geometric Gates in Topological Qubits on NISQ Devices

Matthew Brooks<sup>1,\*</sup>, Foster Sabatino<sup>2,3</sup>, Charles Tahan<sup>1</sup>, and Silas Hoffman<sup>2,4,5,6</sup>

<sup>1</sup>*Department of Physics, University of Maryland, College Park, MD 20740, USA*

<sup>2</sup>*Department of Physics, University of Florida, Gainesville, FL 32611, USA*

<sup>3</sup>*Department of Physics, University of Central Florida, Orlando, FL 32816, USA*

<sup>4</sup>*Quantum Theory Project, University of Florida, Gainesville, FL 32611, USA*

<sup>5</sup>*Laboratory for Physical Sciences, 8050 Greenmead Drive, College Park, Maryland 20740, USA and*

<sup>6</sup>*Condensed Matter Theory Center, Department of Physics, University of Maryland, College Park, MD 20742, USA*

While the adiabatic exchange of Majorana zero modes (MZMs) enables a non-universal set of geometrically protected gates, realising an experimental implementation of MZM braiding remains challenging. In an alternative proposal, charge-parity measurement of two neighboring MZMs supports braiding by teleportation. Moreover, owing to the lack of definitive evidence of MZMs in semiconducting systems, there have been several simulations of MZMs on NISQ devices which more naturally lend themselves to braiding. In this work, measurement-based braiding about MZM Y-junctions are simulated by multi-qubit parity measurements of a logical qubit. Logical single-qubit geometric  $S^{(\dagger)}$  and entangling two-qubit braiding operations are shown using two-physical-qubit joint measurements alone, whilst  $T^{(\dagger)}$ -gates corresponding to a kind of partial-braiding operation, require at least one three-qubit joint measurement. These relatively small scale circuits offer both novel measurement-based geometric gates as well as a measurement-based demonstration of quantum Hamiltonian simulation.

## INTRODUCTION

Non-Abelian anyons, such as Majorana zero modes (MZMs) in solid-state systems, could offer a topologically protected platform with which to process and store quantum information[1, 2]. This is due to the complex phases accrued by anyonic particle exchange, allowing for quantum gate implementation by ordered exchange sequences known as braiding. Despite this promise, isolation and braiding of MZMs remains an experimental challenge[3]. Additionally, proposed operational schemes for MZM quantum processors tend to lack a universal gate set, omitting the elusive  $T$ -gate ( $\pi/4$  phase gate)[4]. Although proposals for the implementation of the  $T$ -gate exist, they lack topological protection[5–9].

An alternative proposal for control of information on a MZM quantum processor is by measurements[10, 11]. This scheme employs joint charge-parity measurements between MZMs coupled by a quantum dot (QD), effectively braiding the MZMs without the need for adiabatic exchange while protecting against quasiparticle-poisoning, the primary source of errors in solid-state MZMs. A notable example of what can be achieved by measurement-based control are geometric phase gates on an encoded four MZM qubit arranged on a Y-junction[12]. This scheme is a measurement-based analogue of the implementation of braided gates[13], and offers robustness against systematic errors that affect the exchange method.

Despite the difficulties in realising topologically protected quantum processors, simulations of topological qubits on NISQ devices have been demonstrated. Such

simulations include non-Abelian anyonic braiding[14–18], topological quantum phase transitions[15, 19–21] and chiral edge states[22]. Although NISQ simulation of charge measurement of non-Abelian anyons has been previously discussed[17], measurement-based control of simulated topological states has not yet been demonstrated.

In this Letter, quantum simulation of non-Abelian anyonic geometric phase gates by measurement are discussed and demonstrated on a superconducting NISQ device. By selecting an appropriate topological gauge with an initial entangled state, sequences of two or more parity measurements implement unitary rotations on the encoded state. Additionally, this concept is shown to scale up to perform entangling braiding operations on two encoded MZM qubits coupled by an additional shared MZM Y-junction. These results constitute the first demonstration of geometric measurement-based quantum computing.

## MODEL

The Hamiltonian of a four-MZM Y-junction is given by

$$H_{\text{MZM}} = 2i\gamma_0(\mathbf{\Delta} \cdot \boldsymbol{\gamma}) \quad (1)$$

where  $\boldsymbol{\gamma} = (\gamma_x, \gamma_y, \gamma_z)$  are the MZMs on each arm of the junction, and  $\mathbf{\Delta} = (\Delta_x, \Delta_y, \Delta_z)$  are the couplings along each arm of the junction[12, 13]. Topologically protected geometric gates with such systems were first derived by sequences of exchange given by the tunable coupling vec-

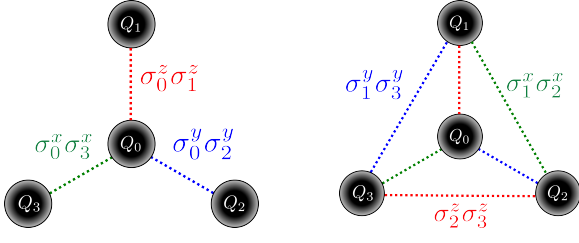


FIG. 1. Qubit analogue of a four MZM Y-junction with Kitaev lattice like connectivity.

tor  $\Delta(\theta, \phi) = |\Delta|(\sin \theta \cos \phi, \sin \theta \sin \phi, \cos \theta)$ . The computational subspace of the qubit comprised of these four MZMs is defined by the ground state  $a|0\rangle = 0$  and excited states  $a^\dagger|0\rangle = |1\rangle$ , with Fermi annihilation (creation) operators are  $a^{(\dagger)} = (\gamma_\theta \pm i\gamma_\phi)/2$  where  $\gamma_i = \gamma \cdot \hat{e}_i$  and  $\hat{e}_i$  is a unit vector defined by the angles associated with an initial coupling vector. By evolving the system couplings so as to trace out an octant on an associated unit sphere of  $\Delta(\theta, \phi)$ , it can be shown that a phase difference between  $|0\rangle$  and  $|1\rangle$  is gathered given by the solid angle of the octant. This is similar to the Berry phase in a spin system. Therefore, by evolving the system so that  $\Delta(0, 0) \rightarrow \Delta(\pi/2, \phi_1) \rightarrow \Delta(\pi/2, \phi_2) \rightarrow \Delta(0, 0)$  traces the solid angle  $\Delta\phi = \phi_2 - \phi_1$ , the phase gate  $R_z(\Delta\phi) = e^{-i\Delta\phi\sigma^z/2}$  is performed on the qubit defined by  $a^{(\dagger)} = (\gamma_{\hat{x}} \pm i\gamma_{\hat{y}})/2$ . This form of the Fermi annihilation (creation) operator is assumed throughout. Here, the total effect of this evolution is to braid  $\gamma_x$  and  $\gamma_y$  in a tunable way, potentially unlocking  $T^{(\dagger)} = R_z(\pm\pi/4)$  operations. Note that  $\text{sgn}(\Delta\phi)$  corresponds to which way around the octant given by  $|\Delta\phi|$  the system is evolved and  $R_z(\Delta\phi)$ .

The same octant may be circumnavigated on the unit sphere by measurements[12]. Charge parity projections between  $\gamma_0$  and each outer MZMs may be generically given by

$$P_{\text{MZM}}(\theta, \phi) = 1 - i\gamma_0 (\gamma_x \sin \theta \cos \phi + \gamma_y \sin \theta \sin \phi + \gamma_z \cos \theta) \quad (2)$$

so by selecting a sequence of measurement axes  $\theta$  and  $\phi$  equivalent to that for the exchange sequence,  $\gamma_x$  and  $\gamma_y$  are braided equivalently and a measurement-based geometric unitary is applied to the system.

Suppose instead of 4 MZMs there are 4 qubits, labeled  $Q_i$  as in Fig. 1(a), also arranged as if on a Y-junction. The interactions along each branch of the MZM Y-junction in (1) may be simulated by the following effective Kitaev lattice Hamiltonian

$$H_{\text{sim}}(\theta, \phi) = \sigma_0^z \sigma_1^z \cos \theta + \sigma_0^y \sigma_2^y \sin \theta \sin \phi + \sigma_0^x \sigma_3^x \sin \theta \cos \phi \quad (3)$$

and projectors simulating those of (2) are given by

$$P_{\pm}(\theta, \phi) = \frac{\mathbb{I} \pm H_{\text{sim}}(\theta, \phi)}{2} \quad (4)$$

where  $\sigma_j^i$  is the  $i^{\text{th}}$  Pauli matrix acting on qubit  $j$ ,  $\mathbb{I}$  is the identity and  $\pm$  dictates measuring the positive or negative eigenstate of the desired observable. Given initialisation to an appropriate logical subspace, a measurement-based geometric phase gate similar to those discussed for a topological system may be demonstrated on a current NISQ processor. A more detailed discussion of this qubitisation method for the Hamiltonian (1) is given in Ref. [18].

An appropriate logical subspace is chosen as orthogonal eigenstates to a chosen set of commuting operators

$$\begin{aligned} W_1 &= \sigma_0^z \sigma_2^x \sigma_3^y & h &= \sigma_0^z \sigma_1^z \\ W_2 &= \sigma_0^x \sigma_1^y \sigma_2^z & n &= \sigma_2^z \sigma_3^z \end{aligned} \quad (5)$$

given from the Hamiltonian of a closed four-mode Kitaev lattice, as depicted in Fig. 1(b). The operators  $W_1$  and  $W_2$  are two of the three integrals of motion of the closed lattice where  $W_3 = n h W_2$ . The operator  $h$  is chosen to set the gauge of the simulated MZM states, and  $n$  differentiates the logical qubit states[18]. The chosen logical states are

$$\begin{aligned} |\tilde{0}\rangle &= \frac{1}{2} (|0101\rangle + |1010\rangle) + \frac{i}{2} (|0110\rangle + |1001\rangle) \\ |\tilde{1}\rangle &= \frac{1}{2} (|0100\rangle + |1011\rangle) - \frac{i}{2} (|0111\rangle + |1000\rangle) \end{aligned} \quad (6)$$

both of which are eigenstates with eigenvalue  $-1$  of  $W_1$ ,  $W_2$  and  $h$  whilst  $|\tilde{0}\rangle$  is an eigenstate with eigenvalue  $-1$  of  $n$  and  $|\tilde{1}\rangle$  is an eigenstate with eigenvalue  $+1$ .

The final ingredient for efficient simulation are logical qubit measurements for state tomography. In the simulated qubit space, the  $z$ -axis of the Bloch sphere is derived from the Fermi operators as  $[a^\dagger, a] = -i\gamma_x \gamma_y$ , therefore defining the  $x$ -axis as  $a + a^\dagger = \gamma_x$  and the  $y$ -axis as  $a - a^\dagger = \gamma_y$ . To translate from the conventional qubit system to the simulated MZM system, we extend the Pauli operators  $\sigma_i^\alpha = i\gamma_i^\alpha \gamma_i$ , where  $u_{ij}^\alpha = i\gamma_i^\alpha \gamma_j^\alpha$  to recover the MZM Hamiltonian (1) by taking  $u_{01}^z = u_{02}^z = u_{03}^z = -1$ . Equally, by taking  $u_{23}^z = -1$ , the gauge and qubit basis operators of simulated system (5), the MZM relations are recovered as  $h \rightarrow i\gamma_0 \gamma_1 \equiv i\gamma_0 \gamma_z$  and  $n \rightarrow i\gamma_2 \gamma_3 \equiv i\gamma_x \gamma_y$  respectively. Therefore, measuring the operator  $n$  is equivalent to measuring along the  $z$ -axis of the simulated Bloch sphere. By extension, with the assumption that the integrals of motion are good quantum numbers  $W_1 = W_2 = -W_3 = -1$  and by application of the identity relation  $-i\sigma_i^x \sigma_i^y \sigma_i^z = \gamma_i^x \gamma_i^y \gamma_i^z \gamma_i$ , it can be shown that the operators  $\sigma_2^y \sigma_3^z \rightarrow \gamma_x$  and  $\sigma_2^x \rightarrow i\gamma_y$ [18]. Thus defining the observables to measure along the  $x$ - and  $y$ -axes of the simulated MZM qubit respectively.

## SINGLE-QUBIT ROTATIONS

### Geometric S-Gate

The Y-junction configuration of the system of interest naturally lends itself to simulation on superconducting NISQ processors with a heavy-hex lattice architecture, such as the *ibm\_brisbane* 127 transmon qubit device. The simplest measurement-based simulation of a MZM geometric gate braiding operation is the  $R_z(\pi/2)$  or  $S$ -gate. This is achieved by the following measurement sequence:  $P_{\pm}(0,0) \rightarrow P_{\pm}(\pi/2,\pi/2) \rightarrow P_{\pm}(\pi/2,0) \rightarrow P_{\pm}(0,0)$ , which is equivalent to  $\sigma_0^z \sigma_1^z \rightarrow \sigma_0^y \sigma_2^y \rightarrow \sigma_0^x \sigma_3^x \rightarrow \sigma_0^z \sigma_1^z$  two-qubit parity checks. Note, the first measurement  $P_{\pm}(0,0)$  may be omitted as it does not perform any rotation on the initial state. This is because alignment along this axis of the unit sphere is provided by correct initialisation.

Two-qubit Pauli matrix parity measurements may be implemented either by entangling the data qubits to an ancilla qubit and measuring the ancilla[23], or by performing a measurement circuit decomposing the two-qubit check into a single-qubit measurement directly on the data qubits. The former allows for all the gate measurements to be performed simultaneously at the cost of greater qubit overhead and potentially circuit depth when limited by the connectivity of a given device. Additionally, the performing the measurements simultaneously will not result in the closed octant of the unit sphere simulated, and thus is not applicable here. The latter is a closer translation of the MZM gate simulated and is a more natural fit for the connectivity of the devices used. Fig. 2 shows the circuit to perform the measurement-based  $S$ -gate simulation without ancillae in standard notation. However, the necessity for mid-circuit measurements means substantial idling time for the qubits not being checked at each step of the gate. Idling errors may be addressed by applying dynamical decoupling pulse sequences, in particular an  $XY - 8$  pulse sequence is used to protect the encoded simulated qubit states.

Unlike in the initial proposal for the measurement base gate in a MZM Y-junction[12], here the measurement outcomes of each parity check are probabilistic. Post-selection could be used to focus on the direct implementation of the gates simulated, given only by measuring the  $-1$  eigenstate for each parity check. However, like in more conventional measurement-based quantum computing methods[24–28], the different possible outcomes of the gate measurements vary the final state only up to known local corrections. These can either be accounted for in-situ with feed-forward single-qubit rotations applied after the measurement sequence, or by calculating separate density matrices for each gate measurement outcome sequence, and applying the appropriate local corrections after-the-fact. For demonstration and charac-

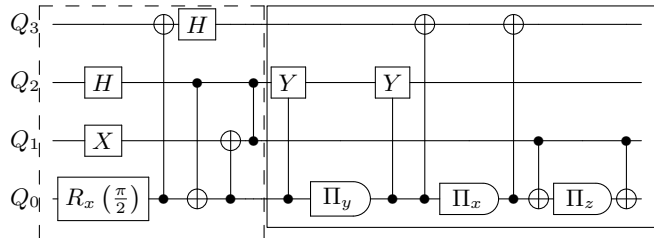


FIG. 2. Circuit to initialise the required  $|\tilde{\uparrow}\rangle$  state (dashed box) with 4 qubits and 2-qubit measurement sequence (solid box) to perform the measurement-based geometric  $S$ -gate in the logical space, and thus simulate a MZM Y-junction operation.  $\Pi_i$  indicates a single qubit measurement on the  $i$ -axis of the Bloch sphere.

terisation of a single measurement-based gate, the latter classical correction method is preferred.

The final ingredient needed to perform the quantum simulations is the choice and preparation of the initial state. While measurements could also be used to initialise the circuits of interest with the knowledge of the gauge choice operator set (5), a gate based approach to state initialisation is simpler and quicker. To demonstrate the geometric measurement-based  $S$ -gate with logical basis state tomography, the  $|\tilde{\uparrow}\rangle = (|\tilde{0}\rangle + |\tilde{1}\rangle)/\sqrt{2}$  is initialised with, as shown in Fig. 2.

As given in Tab. I, on the *ibm\_brisbane* processor, the initial state  $|\tilde{\uparrow}\rangle$  is generated with 89.9% fidelity without and 94.0% fidelity with dynamical decoupling. The measurement-based  $S$ -gate on the same processor returned output state fidelities of  $56.6 \pm 12.0\%$  fidelity without and  $85.7 \pm 3.1\%$  with dynamical decoupling. As predicted, there are substantial improvements in performance both in terms of average fidelity and variance when dynamical decoupling is present. The inverse braiding operation,  $S^\dagger$  or  $R_z(-\pi/2)$ , should consist of the same measurement sequence in reverse:  $P_{\pm_0}(0,0) \rightarrow P_{\pm_1}(\pi/2,0) \rightarrow P_{\pm_2}(\pi/2,\pi/2) \rightarrow P_{\pm_3}(0,0)$  or  $\sigma_0^z \sigma_1^z \rightarrow \sigma_0^x \sigma_3^x \rightarrow \sigma_0^y \sigma_2^y \rightarrow \sigma_0^z \sigma_1^z$ , again, omitting the first measurement. On the same device, the  $S^\dagger$ -gate circuit returned output state fidelities of  $50.7 \pm 7.9\%$  fidelity without and  $85.7 \pm 1.6\%$  with dynamical decoupling. The results of classical simulations of the circuits executed using *qiskit\_aer* simulators are also given in Tab. I. Errors accrued in the simulations stem from imperfect gates and measurements, but not idling errors, and so serve as a useful theoretical upper bound to the fidelities measured on *ibm\_brisbane*. These results suggest that a geometric measurement-based gate and simulation of a topological qubit braiding was achieved with good confidence on a NISQ device.

Operation	Sim	No DD	XY – 8
$ \tilde{\uparrow}\rangle$	98.1%	89.9%	94.0%
$S \tilde{\uparrow}\rangle$	$96.2 \pm 0.6\%$	$56.6 \pm 12.0\%$	$85.7 \pm 3.1\%$
$S^\dagger \tilde{\uparrow}\rangle$	$93.5 \pm 0.4\%$	$50.7 \pm 7.9\%$	$85.7 \pm 1.6\%$
$T \tilde{\uparrow}\rangle$	$71.8 \pm 11.1\%$	$50.5 \pm 5.8\%$	$68.8 \pm 6.7\%$
$T^\dagger \tilde{\uparrow}\rangle$	$75.0 \pm 8.5\%$	$49.7 \pm 5.2\%$	$66.9 \pm 4.9\%$
$ \tilde{00}\rangle$	97.8%	89.8%	89.0%
$R_{xx}(\frac{\pi}{2}) \tilde{00}\rangle$	$90.1 \pm 0.8\%$	$26.1 \pm 2.2\%$	$57.1 \pm 0.9\%$
$R_{xx}(-\frac{\pi}{2}) \tilde{00}\rangle$	$91.3 \pm 1.3\%$	$24.9 \pm 1.9\%$	$70.1 \pm 0.9\%$

TABLE I. Table of output state fidelities measured by logical state tomography for initialisation and measurement-based geometric gate circuits. The *qiskit\_aer* simulated fidelities along with the *ibm\_brisbane* experimental results are given. The experimental results are given both without dynamical decoupling (DD) and with an XY – 8 dynamical decoupling pulse sequence. All experiments consist of 8000 shots with applied measurement error mitigation corrections to the tomography measurements only.

### Geometric T-Gate

The methods demonstrated may be extended to other geometric phase-gates, specifically the elusive  $T^{(\dagger)}$ -gate. With the same encoded logical space, the measurement sequence required to rotate the logical state  $R_z(\tau)$  is  $P_\pm(0,0) \rightarrow P_\pm(\pi/2,0) \rightarrow P_\pm(\pi/2,\tau) \rightarrow P_\pm(0,0)$ . Here the challenge is implementing some for of the 3-qubit measurement

$$P_\pm(\pi/2, \tau) = \frac{\mathbb{I}}{2} \pm \frac{1}{2}(\sigma_0^y \sigma_2^y \cos \tau + \sigma_0^x \sigma_3^x \sin \tau) \quad (7)$$

which cannot be generalised as an observable of the tensor product of three Pauli matrices. The form of the two-qubit parity measurement circuits may be extended to three qubits,

$$P_{3Q}(\tau) = U_{023}(\tau) \left( \frac{\mathbb{I} \pm R_z(\tau) \sigma_0^x R_z^\dagger(\tau)}{2} \right) U_{023}^\dagger(\tau) \quad (8)$$

where  $U_{023}(\tau)$  is some entangling three qubit unitary acting on qubits 0, 2 and 3. The entangling unitary can be written as

$$U_{023}(\tau) = \exp \left[ \frac{i(\pi + 2\tau)}{4} (\mathbb{I} - \sigma_0^z) \left( \mathbb{I} - \frac{\pi \sigma_1^x - 2\tau \sigma_1^x \sigma_2^y}{\pi + 2\tau} \right) \right]. \quad (9)$$

In the case  $\tau = \pi/4$  the  $T$ -gate is implemented. The form of the circuit needed to implement  $U_{023}(\pi/4)$  is given in Fig. 3. Compared to the measurement sequence to implement the  $S^{(\dagger)}$ -gates, the addition of two Toffoli

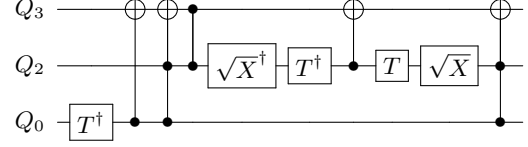


FIG. 3. Quantum circuit implementing  $U_{023}(\pi/4)$ , as is necessary to implement a simulation of the measurement-based geometric  $T^{(\dagger)}$ -gates.

gates and three two-qubit gates each side of the measurement substantially increases the circuit depth. Including the initialisation sequence, the  $T$ -gate circuit is depth 323, compared to a depth of 65 for the  $S$ -gate, when transpiled for the *ibm\_brisbane* processor.

This large circuit depth is felt in the results of measurement-based gate as implemented for the *ibm\_brisbane* processor. With dynamical decoupling a gate fidelity of  $68.8 \pm 6.7\%$  was executed for the  $T$ -gate and a gate fidelity of  $66.9 \pm 4.9\%$  was executed for the  $T^\dagger$ -gate, given by reversing the measurement order as in the  $S^{(\dagger)}$ -gate experiments. This is still relatively close to expected upper bound given by the classically simulated results given in Tab. I.

### GEOMETRIC TWO-QUBIT GATES

Thus far, only measurement-based operations with a single Majorana Y-junction qubits have been considered. The methods discussed may be extended to entangling braiding operations of two such qubits. To do so, along with the two Majorana Y-junctions consisting of four modes each, an additional two modes forming a third Y-junction coupling the two-qubits are required. See Fig. 4 (a). Braiding of MZMs from the two logical qubits is achieved by sequentially measuring the arms of the coupling Y-junction, as in the single-qubit gate operations.

Similarly to the single encoded qubit measurement-based geometric gates simulated with four conventional qubits, entangling operations may be simulated with at least 10 qubits[18]. However, due to the extended geometry of the 10 Majorana mode system, the logical states employed in the single encoded qubit experiments are not applicable. Additionally, the lower symmetry of the three Y-junctions results in asymmetric simulated logical states between the two encoded qubits labeled  $\tilde{Q}_i$  where  $i = 0, 1$ . However, the method of deriving the logical states is the same, by finding eigenstates of the following set of commuting gauge selecting operators derived from the Hamiltonian of the 10 mode closed Kitaev lattice

$$\begin{aligned}
W_1 &= \sigma_0^y \sigma_1^x \sigma_3^z & h_{\tilde{Q}_0} &= \sigma_0^z \sigma_1^z \\
W_2 &= \sigma_0^z \sigma_2^x \sigma_3^y & h_{\tilde{Q}_1} &= \sigma_8^z \sigma_7^z \\
W_3 &= \sigma_7^x \sigma_7^y \sigma_9^z & h_{\mathcal{A}} &= \sigma_4^z \sigma_5^z \\
W_4 &= \sigma_6^y \sigma_7^z \sigma_9^x & n_{\tilde{Q}_0} &= \sigma_2^z \sigma_3^z \\
W_5 &= \sigma_0^x \sigma_1^y \sigma_2^z \sigma_4^y \sigma_5^y & n_{\tilde{Q}_1} &= \sigma_6^z \sigma_9^z,
\end{aligned} \tag{10}$$

where the  $\mp 1$  eigenstates of  $n_{\tilde{Q}_0}$  and  $n_{\tilde{Q}_1}$  define the  $|\tilde{0}\rangle$  ( $|\tilde{1}\rangle$ ) of each encoded qubit respectively. Equally, similarly to the single encoded qubit gates, the operator set (10) defines the operator set used for logical state tomography

$$\begin{aligned}
\sigma_{\tilde{Q}_0}^x &= -i\sigma_2^y \sigma_3^z \sigma_5^z & \sigma_{\tilde{Q}_1}^x &= i\sigma_6^y \\
\sigma_{\tilde{Q}_0}^y &= i\sigma_2^x \sigma_5^z & \sigma_{\tilde{Q}_1}^y &= i\sigma_6^x \sigma_9^z \\
\sigma_{\tilde{Q}_0}^z &= in_{\tilde{Q}_0} & \sigma_{\tilde{Q}_1}^z &= in_{\tilde{Q}_1}.
\end{aligned} \tag{11}$$

The notable difference between this set of measurement operators and the operators used to characterise the single encoded qubit operations is the three qubit measurement  $\sigma_{\tilde{Q}_0}^x$ . The full form of the logical basis states is given in the appendix, along with the circuit for the measurement-based gate investigated here.

The simulated braiding of the two encoded qubits is achieved by an equivalent measurement sequence to the  $S^{(\dagger)}$  gates shown with the single encoded qubit, done on the coupling central Y-junction. Explicitly, by performing a  $\sigma_4^z \sigma_5^z \rightarrow \sigma_4^y \sigma_6^y \rightarrow \sigma_2^x \sigma_4^x \rightarrow \sigma_4^z \sigma_5^z$  parity check sequence, the following entangling operation is implemented

$$R_{xx} \left( \frac{\pi}{2} \right) = \exp \left[ -\frac{i\pi}{4} \left( \sigma_{\tilde{Q}_0}^y \otimes \sigma_{\tilde{Q}_1}^x \right) \right]. \tag{12}$$

Equally, by reversing the measurement sequence, the Hermitian conjugate  $R_{xx} \left( -\frac{\pi}{2} \right)$  is implemented instead. In the MZM picture, this operation is equivalent to braiding the MZMs represented by qubits  $Q_2$  and  $Q_6$  in the qubit analogue show in Fig. (a).

The circuits investigated initialise the logical  $|\tilde{0}\tilde{0}\rangle$  state and implements the  $R_{xx} \left( \pm \frac{\pi}{2} \right)$  measurement sequences. The resulting states are Bell states in the encoded qubit space

$$R_{xx} \left( \pm \frac{\pi}{2} \right) |\tilde{0}\tilde{0}\rangle = \frac{1}{\sqrt{2}} \left( |\tilde{0}\tilde{0}\rangle \mp i |\tilde{1}\tilde{1}\rangle \right). \tag{13}$$

Similarly to to single-qubit gates, these operations are demonstrated on the *ibm\_brisbane* processor, with local corrections due to the gate measurement outcomes corrected with classical post-processing. Output state fidelities are given in Tab.I. Simulations of initialisation

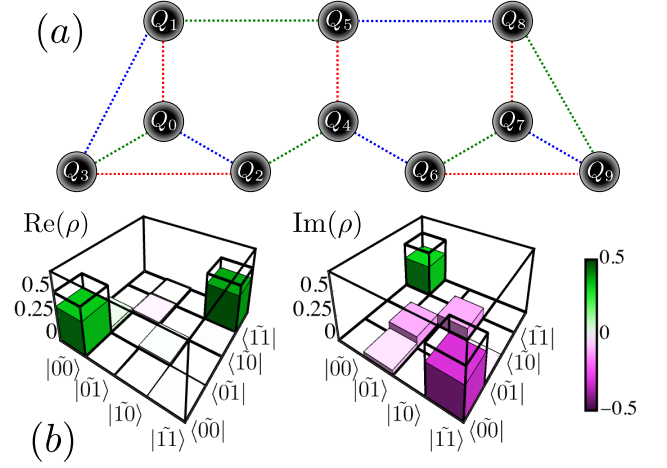


FIG. 4. (a) Qubit analogue of two simulated Majorana Y-junction qubits labeled  $\tilde{Q}_i$  where  $i = 0, 1$ , coupled by two ancilla qubits forming a third intermediate Y-junction labeled  $\mathcal{A}$ . The coloured dashed lines indicate the nature of the coupling between neighbouring qubits in the simulation Hamiltonian, and thus the measurements used to perform operations. Red indicates  $\sigma_i^z \sigma_j^z$ , blue indicates  $\sigma_i^y \sigma_j^y$  and green indicates  $\sigma_i^x \sigma_j^x$ . (b) Density matrix output in the logical subspace of the simulated  $R_{xx} \left( \frac{\pi}{2} \right)$  braiding experiment performed on the *ibm\_brisbane* processor, corresponding to a 70.1% output state fidelity.

and gate fidelities give an expected upper bound in performance of 97.8% and  $91.3 \pm 1.3\%$  respectively. Experiments show output state fidelities up to 89.0% for initialisation,  $57.1 \pm 0.9\%$  for the  $R_{xx} \left( \frac{\pi}{2} \right)$  gate  $70.1 \pm 0.9\%$  for the  $R_{xx} \left( -\frac{\pi}{2} \right)$  gate. The density matrix of the latter result is shown as in Fig. (b). These results demonstrate the successful measurement-based entanglement by braiding of non-Abelian anyonic qubits simulated on a NISQ device.

## CONCLUSION

In this work, the simulation of measurement-based braiding operations of a non-Abelian anyonic qubit described by a four Majorana Y-junction is demonstrated on a NISQ device. By employing sequential two-qubit parity checks in place of charge parity checks on an appropriately initialised state, simulations of the measurement-based geometric  $S^{(\dagger)}$  braiding gates[12] are performed with up to  $\sim 86\%$  output state fidelity. This is extended to show that with the addition of a three qubit non-Pauli measurement, the  $T^{(\dagger)}$  gates may be simulated with up to  $\sim 69\%$  output state fidelity. Finally, entangling operations by the braiding of MZMs from two such anyonic qubits was simulated by sequential measurements around an ancilla Y-junction coupling the two-qubits, with output state fidelity up to  $\sim 70\%$ .

Measurement-based quantum computing is often

discussed for its applications to quantum error correction[23–26], or as device specific realisations of operations on a quantum processor[11, 12, 27, 28]. Here instead, measurement-based quantum simulations have been demonstrated, with little overhead in required qubits, measurements and circuit depths. There is, therefore, scope to scale these simulations to study the effect of measurements on larger anyonic systems such as gapless spin liquids in 2D Kitaev-lattices[29–32]. Finally, the measurement sequences employed in this work are similar to those used in dynamical quantum error correcting codes such as the Floquet code[33–35], and so the simulation techniques outlined here could be used to benchmark such codes.

### ACKNOWLEDGMENTS

We acknowledge helpful discussions with L. Giovia, U. Güngördü, and Y. Yanay. This work is supported by the U.S. Department of Energy, Office of Science, Basic Energy Sciences under Award No. DE-SC0022089.

---

\* matthew.brooks@lps.umd.edu

- [1] A. Y. Kitaev, *Physics-uspekhi* **44**, 131 (2001).
- [2] A. Y. Kitaev, *Annals of physics* **303**, 2 (2003).
- [3] A. Yazdani, F. von Oppen, B. I. Halperin, and A. Yacoby, *Science* **380**, eade0850 (2023).
- [4] S. Bravyi and A. Kitaev, *Physical Review A* **71**, 022316 (2005).
- [5] P. Bonderson, S. D. Sarma, M. Freedman, and C. Nayak, *arXiv preprint arXiv:1003.2856* (2010).
- [6] D. J. Clarke, J. D. Sau, and S. D. Sarma, *Physical Review X* **6**, 021005 (2016).
- [7] S. Hoffman, C. Schrade, J. Klinovaja, and D. Loss, *Physical Review B* **94**, 045316 (2016).
- [8] S. Bravyi, *Physical Review A* **73**, 042313 (2006).
- [9] M. Freedman, C. Nayak, and K. Walker, *Physical Review B* **73**, 245307 (2006).
- [10] Z.-Y. Xue, *The European Physical Journal D* **67**, 1 (2013).
- [11] T. Karzig, C. Knapp, R. M. Lutchyn, P. Bonderson, M. B. Hastings, C. Nayak, J. Alicea, K. Flensberg, S. Plugge, Y. Oreg, *et al.*, *Physical Review B* **95**, 235305 (2017).
- [12] T. Karzig, Y. Oreg, G. Refael, and M. H. Freedman, *Physical Review B* **99**, 144521 (2019).
- [13] T. Karzig, Y. Oreg, G. Refael, and M. H. Freedman, *Physical Review X* **6**, 031019 (2016).
- [14] J. P. Stenger, N. T. Bronn, D. J. Egger, and D. Pekker, *Physical Review Research* **3**, 033171 (2021).
- [15] X. Xiao, J. K. Freericks, and A. F. Kemper, *Quantum* **5**, 553 (2021).
- [16] Google Quantum AI and Collaborators, *Nature* **618**, 264 (2023).
- [17] J. Jovanović, C. Wille, D. Timmers, and S. H. Simon, *arXiv preprint arXiv:2306.13129* (2023).
- [18] F. Sabatino, M. Brooks, C. Tahan, and S. Hoffman, *arXiv preprint arXiv:2503.15405* (2025).
- [19] H.-C. Chang and H.-C. Hsu, *Quantum Information Processing* **21**, 41 (2022).
- [20] R.-Y. Sun, T. Shirakawa, and S. Yunoki, in *2023 IEEE International Conference on Quantum Computing and Engineering (QCE)*, Vol. 2 (IEEE, 2023) pp. 244–245.
- [21] Y.-H. Shi, Y. Liu, Y.-R. Zhang, Z. Xiang, K. Huang, T. Liu, Y.-Y. Wang, J.-C. Zhang, C.-L. Deng, G.-H. Liang, *et al.*, *Physical Review Letters* **131**, 080401 (2023).
- [22] J. M. Koh, T. Tai, and C. H. Lee, *Physical Review Letters* **129**, 140502 (2022).
- [23] G. Üstün, A. Morello, and S. Devitt, *arXiv preprint arXiv:2306.08849* (2023).
- [24] H. J. Briegel, D. E. Browne, W. Dür, R. Raussendorf, and M. Van den Nest, *Nature Physics* **5**, 19 (2009).
- [25] R. Raussendorf and H. J. Briegel, *Physical review letters* **86**, 5188 (2001).
- [26] R. Raussendorf, D. E. Browne, and H. J. Briegel, *Physical review A* **68**, 022312 (2003).
- [27] M. Brooks and C. Tahan, *Physical Review Applied* **16**, 064019 (2021).
- [28] M. Brooks and C. Tahan, *Phys. Rev. B* **108**, 035206 (2023).
- [29] A. Kitaev, *Annals of Physics* **321**, 2 (2006).
- [30] H. Takagi, T. Takayama, G. Jackeli, G. Khaliullin, and S. E. Nagler, *Nature Reviews Physics* **1**, 264 (2019).
- [31] C. Broholm, R. J. Cava, S. Kivelson, D. Nocera, M. Norman, and T. Senthil, *Science* **367**, eaay0668 (2020).
- [32] H. Hu and F. Krüger, *Physical Review Letters* **133**, 146603 (2024).
- [33] M. B. Hastings and J. Haah, *Quantum* **5**, 564 (2021).
- [34] M. Davydova, N. Tantivasadakarn, and S. Balasubramanian, *PRX Quantum* **4**, 020341 (2023).
- [35] A. Paetznick, C. Knapp, N. Delfosse, B. Bauer, J. Haah, M. B. Hastings, and M. P. da Silva, *PRX Quantum* **4**, 010310 (2023).

## 10 Qubit Circuit

The logical basis states for the simulation of the 10 MZM system encoding two topological qubits, as derived from the set of operators in Eq. 10 are

$$\begin{aligned}
|0\rangle_{\tilde{Q}_0} &= \frac{\sqrt{2}}{4} (|010101\rangle + |010110\rangle + |101001\rangle + |101010\rangle) + \frac{i\sqrt{2}}{4} (|011001\rangle + |011010\rangle + |100101\rangle + |100110\rangle) \\
|1\rangle_{\tilde{Q}_0} &= -\frac{\sqrt{2}}{4} (|011101\rangle - |011110\rangle + |100001\rangle - |100010\rangle) - \frac{i\sqrt{2}}{4} (|010001\rangle - |010010\rangle + |101101\rangle - |101110\rangle) \\
|0\rangle_{\tilde{Q}_1} &= \frac{\sqrt{2}(i+1)}{4} (|0110\rangle + |1001\rangle) - \frac{\sqrt{2}(i-1)}{4} (|0101\rangle + |1010\rangle) \\
|1\rangle_{\tilde{Q}_1} &= \frac{\sqrt{2}(i-1)}{4} (|0111\rangle + |1000\rangle) - \frac{\sqrt{2}(i+1)}{4} (|0100\rangle + |1011\rangle).
\end{aligned} \tag{14}$$

The full circuit to perform the  $R_{xx}(\frac{\pi}{2})$  simulated braiding gates on the logical input state  $|\tilde{00}\rangle$  is given in Fig. 5. Note that to perform a  $R_{xx}(-\frac{\pi}{2})|\tilde{00}\rangle$  simu-

lated braiding gates, one need only re-arrange the order of measurements.

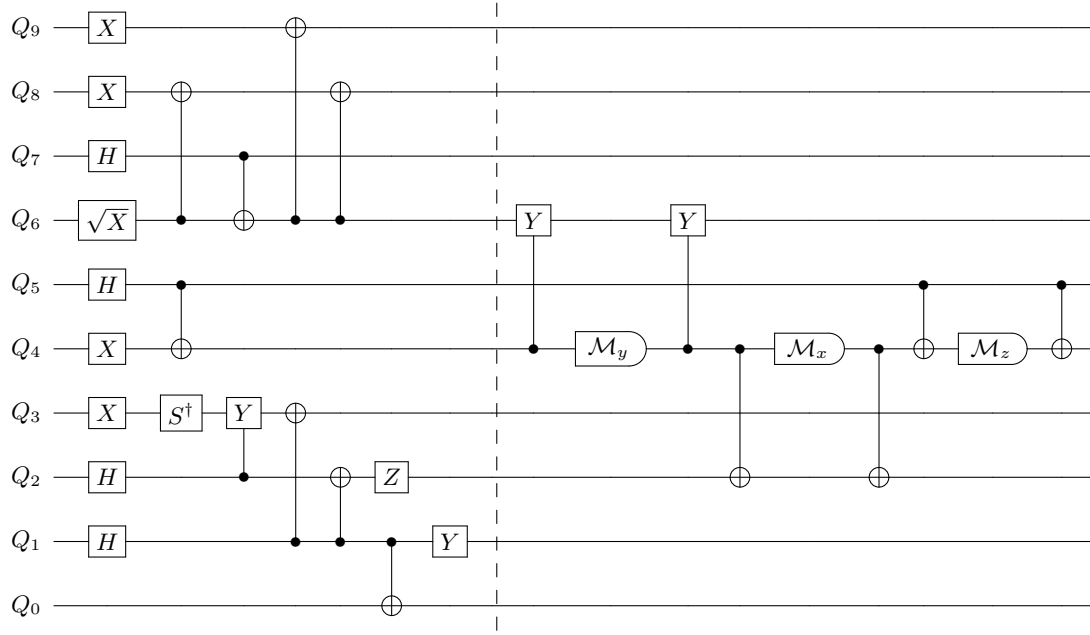


FIG. 5. 10 qubit circuit to perform the  $R_{xx}(\frac{\pi}{2})|\tilde{00}\rangle$  simulated braiding gate. To the left of the dashed barrier is the simulation basis initialisation circuit, to the right is the sequence of measurements responsible for the simulated rotation. The qubit labels  $Q_i$  correspond to the qubit layout given in Fig. 4.